Supplementary Information

Fabrication of novel ternary g-C_3N_4/$Zn_{0.5}Ni_{0.5}Fe_{1.8}Mn_{0.2}O_4$/rGO hybrid nanocomposites for humidity sensing

Moksodur Rahman[a], Md. Lutfor Rahman[*,a], Bristy Biswas[a], Md. Farid Ahmed[a], Md. Aftab Ali Shaikh[a,b], Shirin Akter Jahan[a], Nahid Sharmin[a]

[a]Institute of Glass and Ceramic Research and Testing (IGCRT), Bangladesh Council of Scientific and Industrial Research (BCSIR), Dhanmondi, Dhaka-1205, Bangladesh.

[b]Department of Chemistry, University of Dhaka, Dhaka-1000, Bangladesh

*Corresponding Author: lutforrahman@bcsir.gov.bd; lutforju33@yahoo.com

1. Synthesis of Graphene Oxide (GO)

In a standard synthesis procedure, 3.5 grams of graphite and 1.75 grams of sodium nitrate were dispersed in 100 milliliters of concentrated (98%) sulfuric acid. The mixture was cooled to approximately 5 °C using an ice bath and stirred continuously for 2.5 hours. Subsequently, over the course of another 2.5 hours, 12 grams of potassium permanganate were gradually added while maintaining constant stirring for an additional 2 hours. After this, the ice bath was removed, allowing the mixture to warm to room temperature.

Following this, about 120 milliliters of distilled water were slowly added over one hour, during which gas evolution was observed, and the temperature was increased to around 90 °C using a water bath. Once the temperature reached 90 °C, an extra 320 milliliters of water were introduced, and the mixture was stirred continuously for 1.5 hours to form a mud-brown suspension. This suspension was then treated with 30% hydrogen peroxide (H_2O_2), and approximately 4 liters of warm distilled water were added to dilute the mixture. The precipitate was allowed to settle under gravity for 24 hours, after which the clear supernatant was carefully decanted.

To remove excess manganese and sulfate ions, 2 M hydrochloric acid (HCl) was added to the mixture. The resulting suspension was repeatedly washed using high-speed centrifugation and distilled water until a neutral pH of around 7 was achieved. Finally, the GO was obtained by filtration and stored in a vacuum desiccator over silica gel for several days prior to characterization and use in composite materials.

2. From PXRD data, the peak profile analysis carried out by following parameters:

The average crystallite sizes were measured using following classical Scherrer ($D_{C\text{-}S}$) method [1]:

$$D_{C-S} = 0.9\lambda/(\beta_{hkl} \cdot cos\theta) \quad (1)$$

Where, λ equal to X-ray wavelength, β_{hkl} is the full width at half maximum (FWHM) intensity of the respective miller indices and θ equivalents to Bragg angle.

Munshi-Scherrer equation also obtained by rearranging Eq. (1) and taking logarithm on both sides as follows [2]:

$$ln\beta_{hkl} = ln\left({}^{0.9\lambda}/_{D_{M-S}}\right) + ln\left({}^{1}/_{cos\theta}\right) \quad (2)$$

$$D_{M-S} = 0.9\lambda/e^{intercept} \quad (3)$$

With the help of Eq. (2) and (3) crystallite size was calculated using intercept, which obtained by linear plot of ln(1/cosθ) along X-axis and lnβ along Y-axis.

The average crystallite size also estimated using Williamson-Hall (W-H) model [2].

$$\mathrm{B}_{hkl} \cdot cos\theta = 0.9\lambda/D_{W-H} + 4\varepsilon \cdot sin\theta \quad (4)$$

The intercept of the fitted line will be obtained by linear plot of βcosθ along Y-axis and 4sinθ along X-axis. Crystallite size estimated from intercept using Eq. (5) as follows:

$$D_{W-H} = 0.9\lambda/intercept \quad (5)$$

The Size-Strain Plot (SSP) model also used to evaluate the crystallite size by following Equations (6-7) [3].

$$\left(D_{hkl}\beta_{hkl}cos\theta\right)^2 = {}^{k\lambda}/_{D}\left(d_{hkl}^2\beta_{hkl}cos\theta\right) + \left({}^{\varepsilon}/_{2}\right)^2 \quad (6)$$

$$D_{SSP} = \ 0.9\lambda/Slope \quad (7)$$

The slope of the fitted line will be obtained by plot of $(d\beta\cos\theta)^2$ with respect to $(d^2\beta\cos\theta)$, which gives the crystallite size .

Halder-Wagner model is another technique which gives crystallite size precisely by given Eq. (8)[4]:

$$\left({}^{\beta_{hkl}}/_{tan\theta}\right)^2 = \left({}^{k\lambda}/_{D_{H-W}}\right)\left({}^{\beta_{hkl}}/_{tan\theta\ cos\theta}\right) + 16\varepsilon^2 \qquad (8)$$

A linear fit graph is made by plotting of $(\beta_{hkl}/\tan\theta)^2$ versus $(\beta_{hkl}/\tan\theta\cos\theta)$ and obtained slope gives Halder-Wagner crystallite size.

Lattice constant 'a' was calculated using Eq. (9)

$$a = d_{hkl}\sqrt{h^2 + k^2 + l^2} \qquad (9)$$

Surface area and lattice strain (ε) of the prepared sample was estimated using the following Eq. 10-11 [5].

$$S = 6/D_{C-S} \cdot \varrho_x \qquad (10)$$

$$\varepsilon = \beta_{hkl}/tan\theta \qquad (11)$$

The x-ray density (ϱ_x) was calculated from the values of the lattice parameter using the following relation [5]:

$$\varrho_x = {}^{8M}/_{Na^3} \qquad (12)$$

where 8 signifies the number of molecules in a unit cell of spinel ferrites lattice. M, N and a is molecular weight, Avogadro's number, and the lattice parameter, respectively.

The Bulk density (ϱ_b) were calculated from the values of pellets parameter by using the following equation [6]:

$$\varrho_b = m/\pi r^2 t \quad (13)$$

Where, m, r, and t is the weight, radius, and thickness of pellets respectively.

The percentage porosity (P) of the samples was determined using the formula:

$$P = 1 - \left({bulk\ density}/{x - ray\ density}\right) \quad (14)$$

By using PXRD data various tetrahedral (A-sites) and octahedral (B-sites) parameter such as ionic radii (Ir_A, Ir_B), bond length (BL_{A-O}, BL_{B-O}), and hoping length (HL_A, HL_B) also calculated using Eq. (15-16), (17-18), and (19-20), respectively [7–9].

$$Ir_A = \left(u - {1}/{4}\right)a\sqrt{3} - r(O^{2-}) \quad (15)$$

$$Ir_B = \left({5}/{8} - u\right)a - r(O^{2-}) \quad (16)$$

$$Bond\ length, BL_{A-O} = \left(u - {1}/{4}\right)a\sqrt{3} \quad (17)$$

$$Bond\ length, BL_{B-O} = \left({5}/{8} - u\right)a \quad (18)$$

$$HL_A = a\sqrt{3}/4 \quad (19)$$

$$HL_B = a\sqrt{2}/4 \quad (20)$$

where *a* denotes the lattice constant, $r(O^{2-})$ signifies the radius of the oxygen ion (0.135 nm), and *u* is the oxygen ion parameter (0.375) for an ideal spinel ferrite.

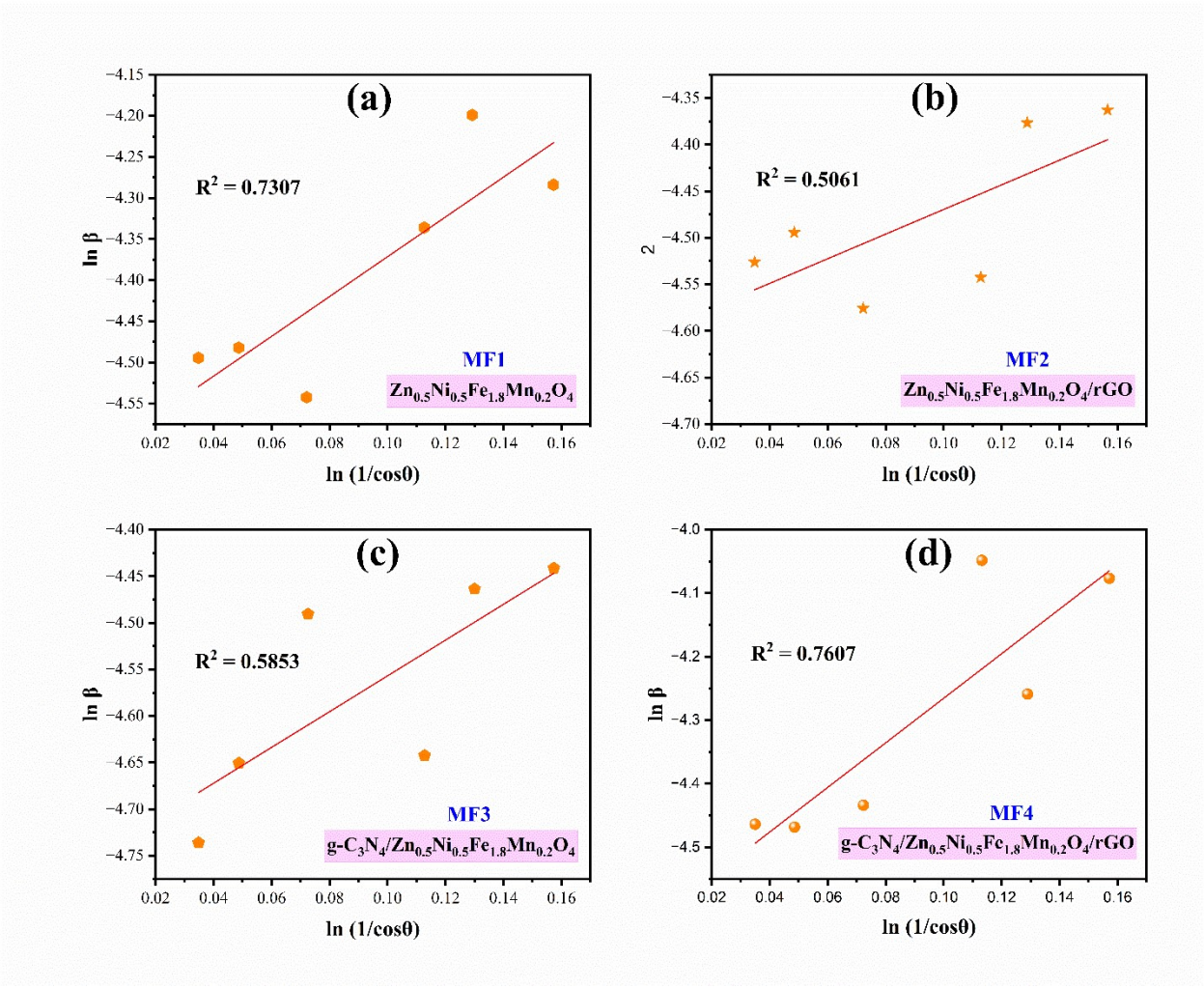

Figure S1: Munshi-Scherrer plots of (a) $Zn_{0.5}Ni_{0.5}Fe_{1.8}Mn_{0.2}O_4$, (b) $Zn_{0.5}Ni_{0.5}Fe_{1.8}Mn_{0.2}O_4$/rGO, (c) g-$C_3N_4$/$Zn_{0.5}Ni_{0.5}Fe_{1.8}Mn_{0.2}O_4$, (d) g-$C_3N_4$/$Zn_{0.5}Ni_{0.5}Fe_{1.8}Mn_{0.2}O_4$/rGO

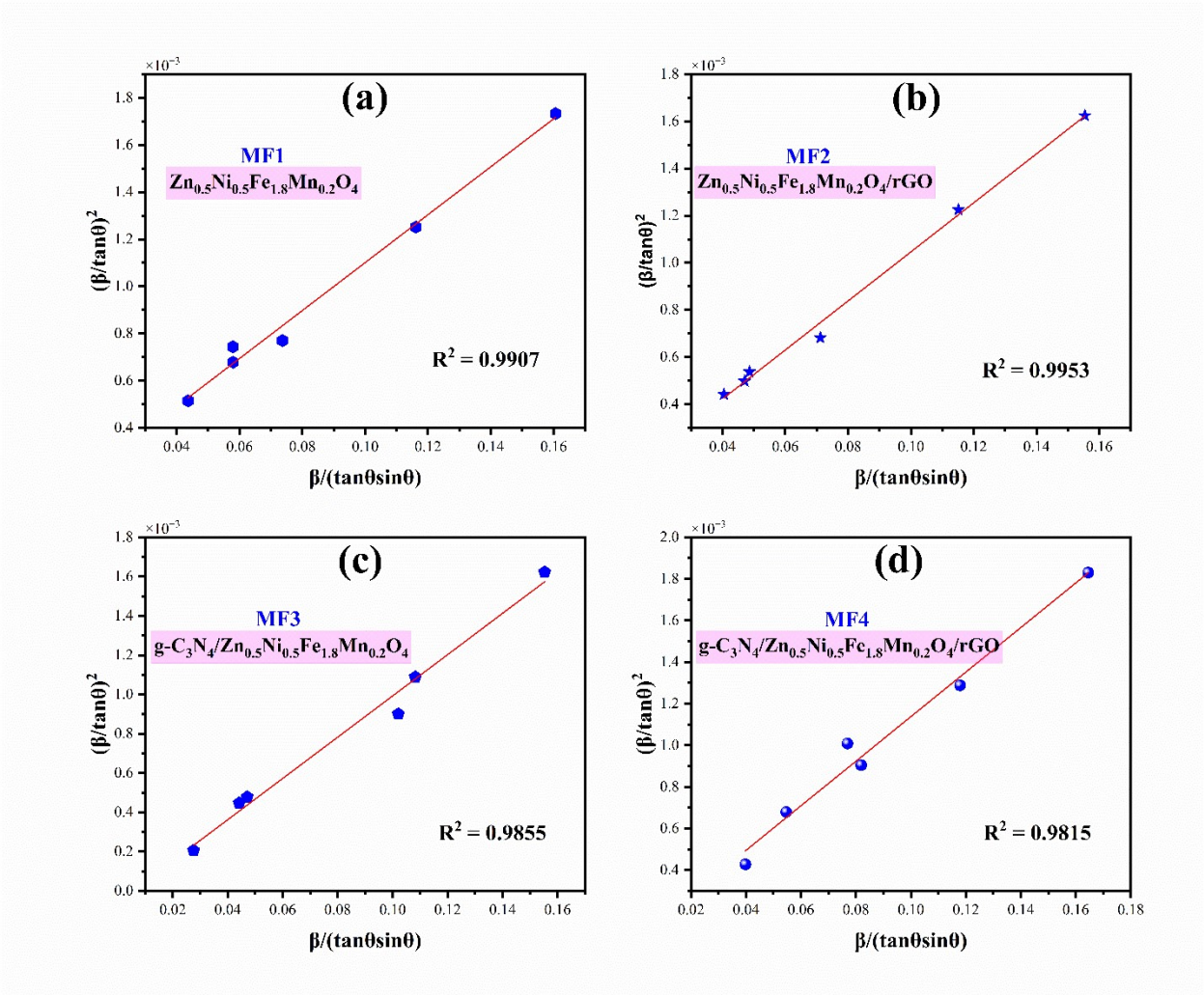

Figure S2: Size-Strain plots of (a) $Zn_{0.5}Ni_{0.5}Fe_{1.8}Mn_{0.2}O_4$, (b) $Zn_{0.5}Ni_{0.5}Fe_{1.8}Mn_{0.2}O_4$/rGO, (c) g-$C_3N_4$/$Zn_{0.5}Ni_{0.5}Fe_{1.8}Mn_{0.2}O_4$, (d) g-$C_3N_4$/$Zn_{0.5}Ni_{0.5}Fe_{1.8}Mn_{0.2}O_4$/rGO

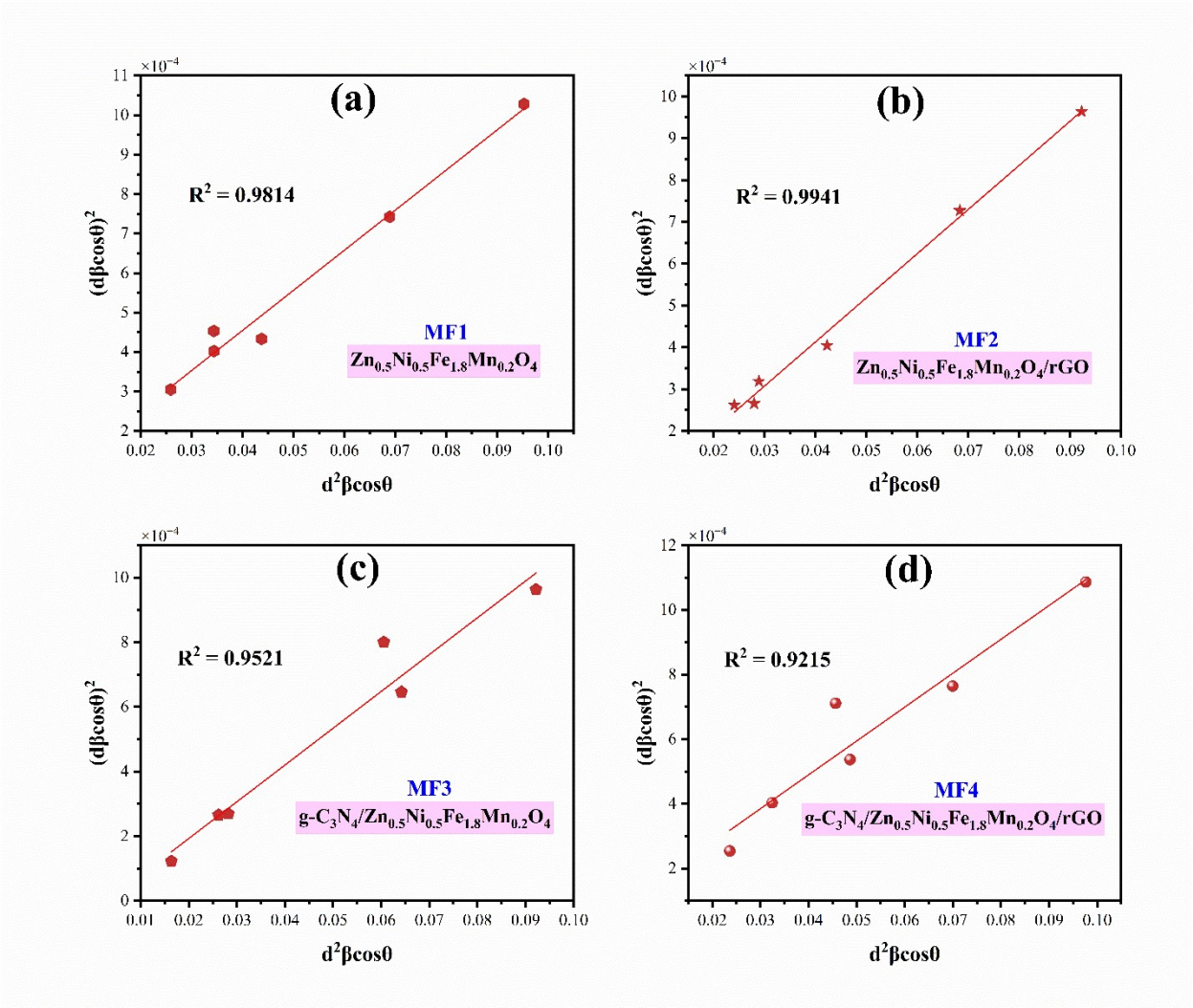

Figure S3: Halder-Wagner plots of (a) $Zn_{0.5}Ni_{0.5}Fe_{1.8}Mn_{0.2}O_4$, (b) $Zn_{0.5}Ni_{0.5}Fe_{1.8}Mn_{0.2}O_4$/rGO, (c) g-$C_3N_4$/$Zn_{0.5}Ni_{0.5}Fe_{1.8}Mn_{0.2}O_4$, (d) g-$C_3N_4$/$Zn_{0.5}Ni_{0.5}Fe_{1.8}Mn_{0.2}O_4$/rGO

3. Humidity chamber

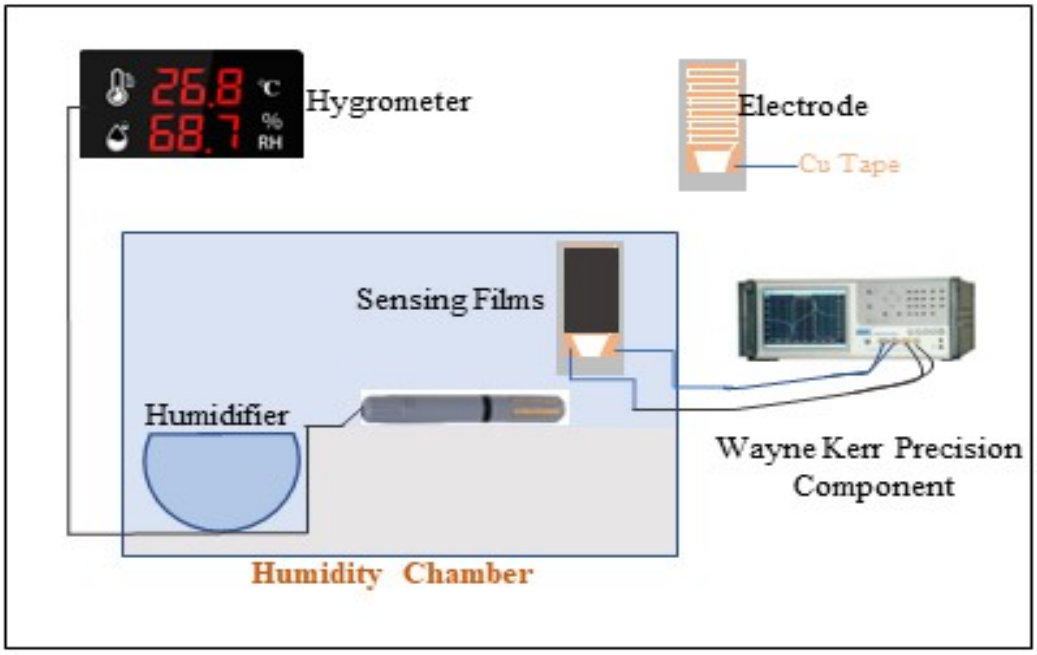

Figure S4: Fabricated closed humidity measurement chamber

4. XPS spectra of MF4

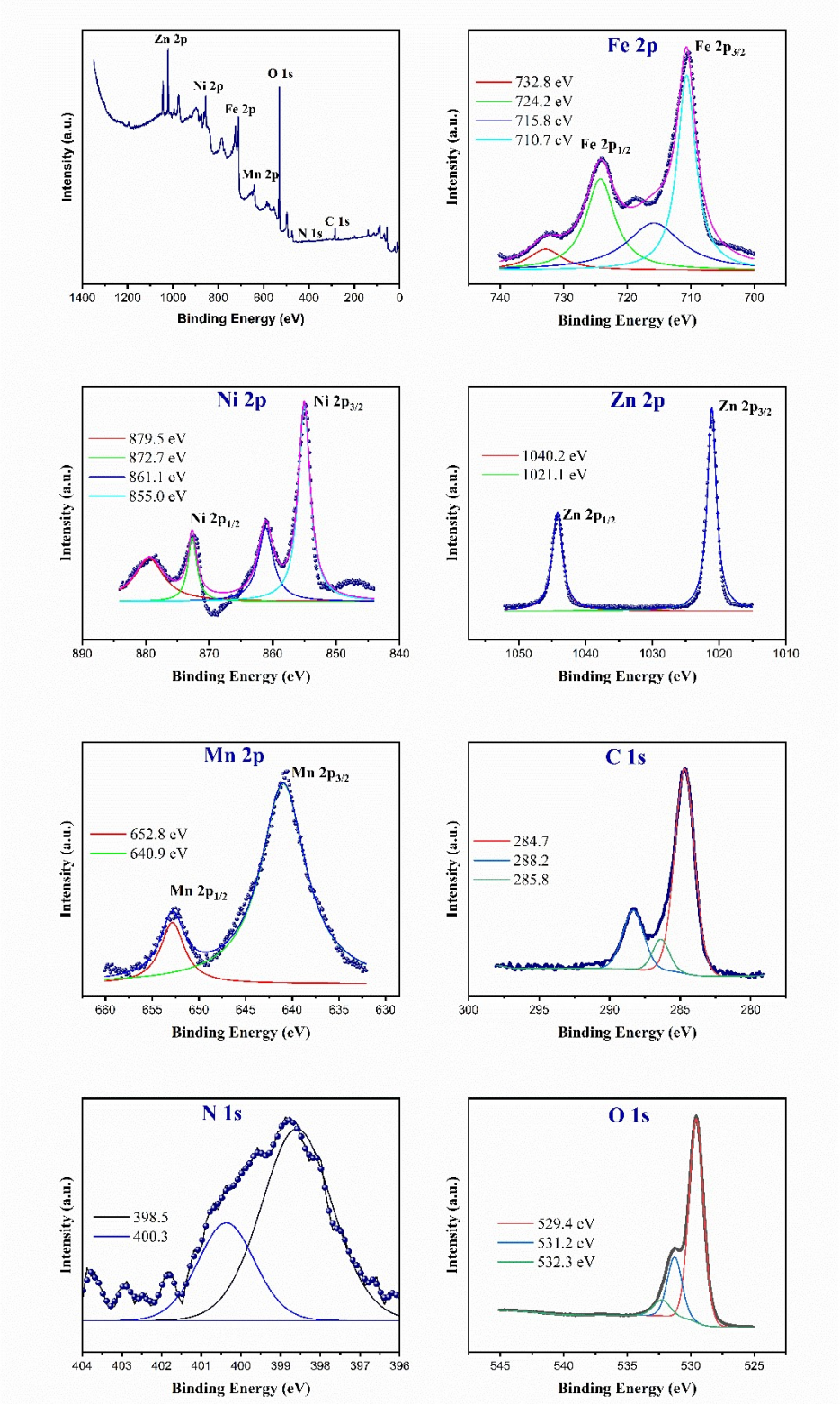

Figure S5. XPS spectra of Zn, Ni, Fe, Mn, C, N, and O in MF4 nanocomposites.

5. FTIR spectra of g-C_3N_4, GO, and rGO

Figure S6 depicts the FTIR spectra of **g-C_3N_4.** The peaks observed in the region between 1200–1600 cm^{-1} are characteristic of the C-N heterocycles and C=N stretching modes present in the g-C_3N_4 structure. This region signifies the core features of graphitic carbon nitride. Additionally, the broad peak around 3000–3500 cm^{-1} is indicative of N-H stretching, which may arise from residual amino groups or adsorbed water molecules. The strong absorption around 800 cm^{-1} is attributed to the out-of-plane bending of heptazine units, confirming the unique framework of g-C_3N_4 [1–4].

Figure S6 depicts the FTIR spectra of GO. For graphene oxide (GO), the spectrum highlights the presence of various oxygen-containing functional groups. A broad band between 3200–3500 cm^{-1} corresponds to O-H stretching vibrations, indicating the presence of hydroxyl groups and possibly adsorbed water. The peak around 1700 cm^{-1} is associated with C=O stretching, likely from carboxyl or ester groups present in GO. Peaks in the range of 1400–1600 cm^{-1} are linked to C=C stretching, showing that some degree of the sp^2-hybridized carbon network remains intact. Additional peaks between 1100–1300 cm^{-1} can be attributed to C-O stretching vibrations, which represent epoxide or hydroxyl functionalities on the GO surface [5,6].

Figure S6 depicts the FTIR spectra of rGO. In the spectrum of reduced graphene oxide (rGO), fewer peaks are observed, indicating a reduction in the number of oxygen-containing groups. The intensity of the O-H stretching band near 3200 cm^{-1} is significantly reduced, confirming the successful removal of hydroxyl and epoxide groups during the reduction process. The C=O stretching peak near 1700 cm^{-1} also weakens, suggesting the reduction or elimination of carbonyl groups in rGO. The C=C stretching band around 1600 cm^{-1} becomes more pronounced, reflecting the restoration of the sp^2-hybridized carbon network as a result of the reduction. Moreover, the peaks associated with C-O bonds between 1100–1300 cm^{-1} are either diminished or completely eliminated, further verifying the reduction of oxygen-containing groups in rGO [5–8].

This comparison between the GO and rGO spectra underscores the significant reduction in oxygen functionalities during the transition from GO to rGO. The attenuation of peaks related to hydroxyl, carboxyl, and epoxide groups, along with the reappearance of a strong C=C signal, highlights the restoration of the conjugated carbon network, crucial for enhanced electrical conductivity and material properties in rGO.

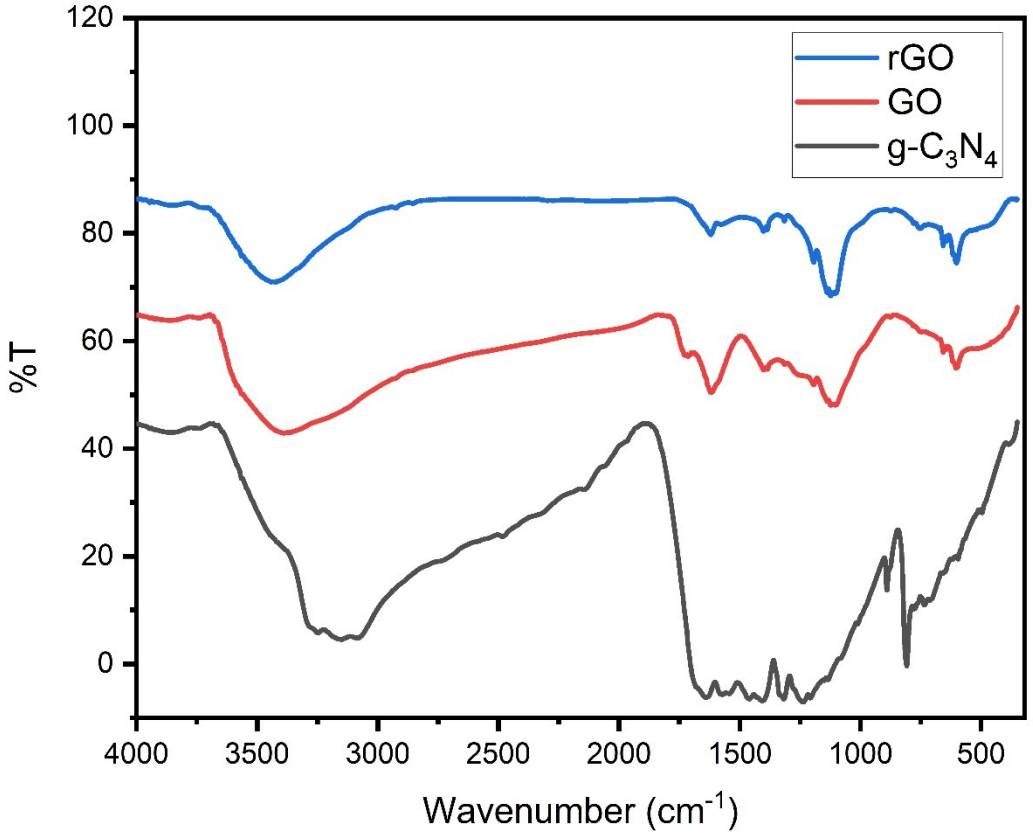

Figure S6: FT-IR spectra of g-C_3N_4, GO, and rGO

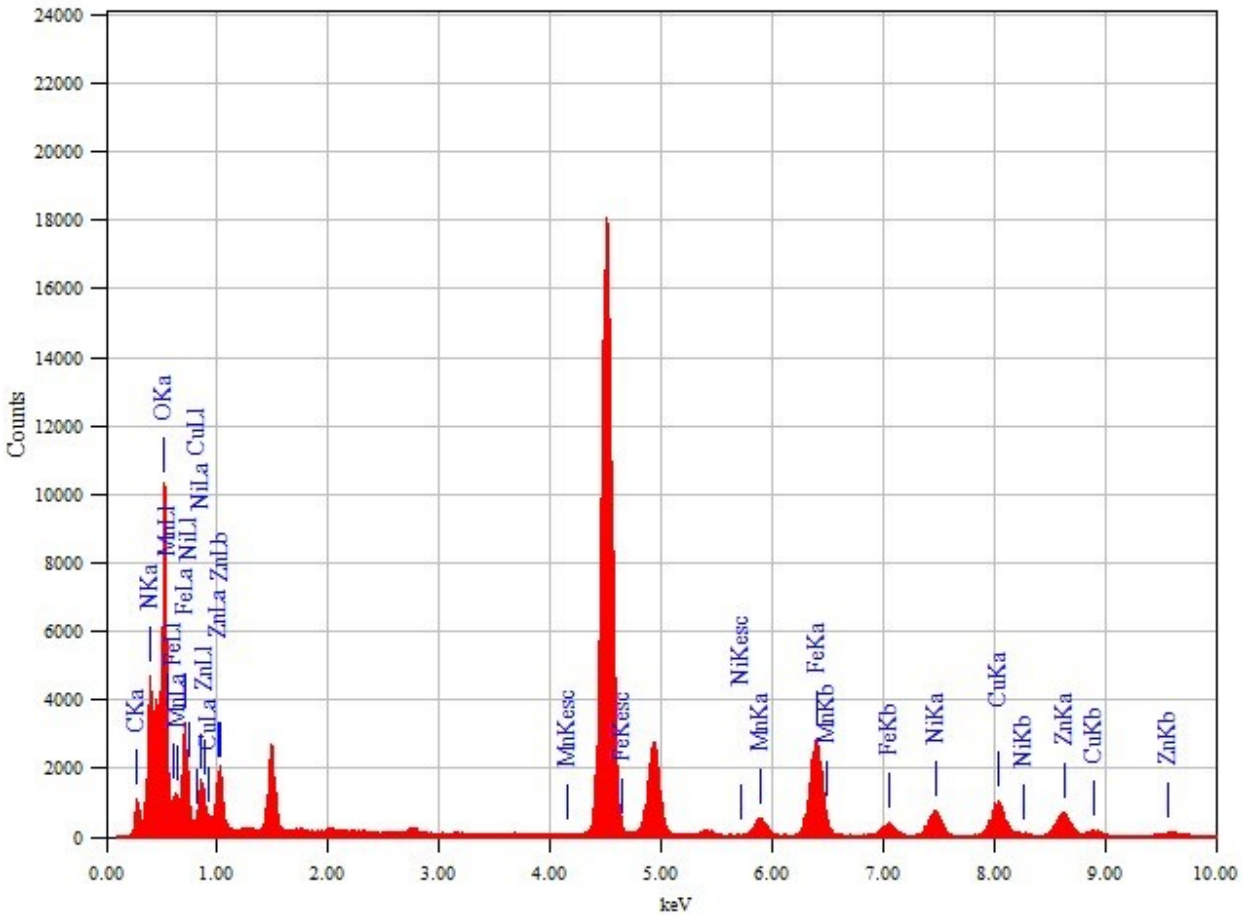

Figure S7: EDS spectra of MF4

Reference:

[1] N. Boonprakob, N. Wetchakun, S. Phanichphant, D. Waxler, P. Sherrell, A. Nattestad, J. Chen, B. Inceesungvorn, Enhanced visible-light photocatalytic activity of g-C3N4/TiO2 films, J Colloid Interface Sci 417 (2014) 402–409. https://doi.org/10.1016/j.jcis.2013.11.072.

[2] P.B. Koli, M.D. Birari, S.A. Ahire, S.G. Shinde, R.S. Ingale, I.J. Patil, Ferroso-ferric oxide (Fe3O4) embedded g-C3N4 nanocomposite sensor fabricated by photolithographic technique for environmental pollutant gas sensing and relative humidity characteristics, Inorg Chem Commun 146 (2022). https://doi.org/10.1016/j.inoche.2022.110083.

[3] B. Zhu, P. Xia, W. Ho, J. Yu, Isoelectric point and adsorption activity of porous g-C 3 N 4, Appl Surf Sci 344 (2015) 188–195. https://doi.org/10.1016/j.apsusc.2015.03.086.

[4] X. Yang, F. Qian, G. Zou, M. Li, J. Lu, Y. Li, M. Bao, Facile fabrication of acidified g-C3N4/g-C3N4 hybrids with enhanced photocatalysis performance under visible light irradiation, Appl Catal B 193 (2016) 22–35. https://doi.org/10.1016/j.apcatb.2016.03.060.

[5] G. Surekha, K.V. Krishnaiah, N. Ravi, R. Padma Suvarna, FTIR, Raman and XRD analysis of graphene oxide films prepared by modified Hummers method, in: J Phys Conf Ser, Institute of Physics Publishing, 2020. https://doi.org/10.1088/1742-6596/1495/1/012012.

[6] B.D. Ossonon, D. Bélanger, Synthesis and characterization of sulfophenyl-functionalized reduced graphene oxide sheets, RSC Adv 7 (2017) 27224–27234. https://doi.org/10.1039/c6ra28311j.

[7] M. Strankowski, D. Włodarczyk, Ł. Piszczyk, J. Strankowska, Polyurethane Nanocomposites Containing Reduced Graphene Oxide, FTIR, Raman, and XRD Studies, Journal of Spectroscopy 2016 (2016). https://doi.org/10.1155/2016/7520741.

[8] T. Rattana, S. Chaiyakun, N. Witit-Anun, N. Nuntawong, P. Chindaudom, S. Oaew, C. Kedkeaw, P. Limsuwan, Preparation and characterization of graphene oxide nanosheets, in: Procedia Eng, Elsevier Ltd, 2012: pp. 759–764. https://doi.org/10.1016/j.proeng.2012.02.009.